The unfolded protein response governs integrity of the human hematopoietic stem cell pool during stress

Authors: Peter van Galen[1], Antonija Kreso[1], Nathan Mbong[1], Erno Wienholds[1], David G. Kent[2], Timothy Fitz-Maurice[3], Joseph E. Chambers[2], Stephanie Xie[1], Elisa Laurenti[1], Karin Hermans[1], Kolja Eppert[4], Stefan J. Marciniak[2], Jane C. Goodall[3], Anthony R. Green[2], Bradly G. Wouters[1], John E. Dick[1]

Affiliations:

[1] Princess Margaret Cancer Centre, University Health Network and Department of Molecular Genetics, University of Toronto, Ontario, Canada.

[2] Cambridge Institute for Medical Research, Wellcome Trust/MRC Stem Cell Institute and Department of Haematology, University of Cambridge, Cambridge, United Kingdom

[3] University of Cambridge, Department of Medicine, Cambridge, United Kingdom

[4] Department of Pediatrics, McGill University, Montreal Children's Hospital Research Institute, Westmount, Quebec, Canada.

Correspondence should be addressed to:

John E. Dick

Senior Scientist, Princess Margaret Cancer Centre, University Health Network.

Professor, Dept. of Molecular Genetics, University of Toronto.

Director, Program in Cancer Stem Cells, Ontario Institute for Cancer Research.

Office: Rm 8-354, Toronto Medical Discovery Tower, 101 College St. Toronto, M5G2C1.

Phone: 416-581-7472.

Email: jdick@uhnres.utoronto.ca

The blood system is sustained by a pool of hematopoietic stem cells (HSC) that are long-lived due to their capacity for self-renewal. A consequence of longevity is exposure to stress stimuli including reactive oxygen species (ROS), nutrient fluctuation, and DNA damage[1,2]. Damage that occurs within stressed HSC must be tightly controlled to prevent either loss of function or the clonal persistence of oncogenic mutations that increase the risk of leukemogenesis[3,4]. Despite the importance of maintaining cell integrity throughout life, how the HSC pool achieves this and how individual HSC respond to stress remains poorly understood. Many sources of stress cause misfolded protein accumulation in the endoplasmic reticulum (ER) and subsequent activation of the unfolded protein response (UPR) that enables the cell to either resolve the stress or initiate apoptosis[5,6]. Here we show that human HSC are predisposed to UPR mediated apoptosis compared to closely related early progenitors (EP). Following ER stress in HSCs, the PERK branch of the UPR is strongly activated, causing ATF4, *CHOP* and *GADD34* upregulation leading to apoptosis. In contrast, EP exhibit an adaptive response to stress leading to their survival. Modulation of UPR signaling in HSC by overexpression of the co-chaperone ERDJ4 increases HSC repopulation capacity in xenograft assays, directly linking the UPR to HSC function. Since the UPR is a focal point where different sources of stress converge, our study provides a framework for understanding how stress signaling is coordinated within the hematopoietic hierarchy and integrated with stemness. Moreover, our results may open up an avenue to exploit UPR signaling as a means to improve clinical transplantation of HSC. More broadly, these findings reveal how various sources of stress lead to clearance of individual HSC to prevent propagation of damaged HSC providing insight into how the stem cell pool maintains clonal integrity.

The human hematopoietic hierarchy has recently been delineated at the single cell level, enabling precise isolation of HSC and progenitor cells (HSPC)[7-9] (Supplementary Table 1). We performed pathway analysis using the gene expression signature of highly purified HSC from lineage depleted cord blood (CB)[10], and identified components of the UPR to be enriched in HSC compared to progenitor cells (Fig. 1a-b). The UPR encompasses the IRE-1, PERK and ATF6 pathways[6] (Supplementary Fig. 1a). Quantitative PCR showed that several genes of the PERK signaling branch were more highly expressed in $CD34^+CD38^-$ (HSPC) compared to $CD34^+CD38^+$ (EP) fractions: *PERK* (1.8-fold), *ATF4* (1.5-fold) and its transcriptional targets *XBP1* (2.3-fold), *ERDJ4* (2.1-fold) and *CHOP* (1.7-fold), and the *CHOP* targets *GADD34* (1.3-fold) and *ERO1LB* (2.1-fold, Fig. 1c, Supplementary Fig. 1b-e, Supplementary Table 2). HSPC-enriched expression of *CHOP* and *ERDJ4* was also seen in adult bone marrow (BM, Supplementary Fig. 1f). As well, expression of *ATF6* and the ER resident chaperone *GRP94* was enriched in CB HSPC compared to EP (Fig. 1d-e). However, splicing of *XBP1* mRNA, which is representative of IRE1 activity, was lower in HSPC compared to EP (2.8-fold, Fig. 1f). Taken together, gene expression analysis of HSPC and EP fractions suggests differential activation of UPR branches, with increased expression of PERK dependent genes and decreased activity of IRE-1 in HSC.

To examine whether differential basal UPR gene expression reflects distinct ER stress responses in HSC and EP, we used two chemical inducers of ER stress, Thapsigargin (Tg) and Tunicamycin (Tm). Tg disrupts Ca^{2+} homeostasis by inhibiting SERCA in the ER membrane, depleting Ca^{2+} from the ER and rapidly activating all three branches of the UPR[11]. Treatment of sorted HSPC and EP with Tg resulted in upregulation of the canonical UPR target genes *GRP94*, *GRP78* and *ERDJ4* (Fig. 1g, Supplementary Fig. 2a). Interestingly, after 30 minutes, the ratio of

spliced over total *XBP1* was increased by 9.0±1.1 fold in EP but only 2.4±0.3 fold in HSPC cells (Fig. 1g). The level of *XBP1* splicing was diminished after 6 hours, consistent with quick attenuation of IRE-1 activity[12]. This indicates that differential *XBP1* splicing between HSC and EP under steady state conditions is exaggerated upon Tg-induced ER stress, consistent with repressed IRE-1 pathway activity in HSC.

Tm blocks synthesis of N-linked glycoproteins, causing accumulation of unfolded proteins in the ER[11]. Tm treatment resulted in higher upregulation of the canonical UPR genes *GRP94*, *GRP78* and *ERDJ4* in HSPC compared to EP (Fig. 1h, Supplementary Fig. 2b). The level of *XBP1* splicing by the IRE1 branch of the UPR was not different between CB-derived HSPC and EP following Tm treatment. In contrast, the PERK pathway target *CHOP* was more upregulated in HSPC compared to EP following addition of 0.6 µg/mL Tm (HSPC: 21±1.8-fold, EP: 5.9±0.4-fold, Fig. 1h). As well, *ATF4* (HSPC: 2.1±0.1-fold, EP: 1.4±0.04-fold) and *GADD34* (HSPC: 6.2±0.4-fold, EP: 1.8±0.2-fold) were more upregulated in HSPC compared to EP (Supplementary Fig. 2b). In adult BM, upregulation of PERK pathway target genes was less dramatic, but *CHOP* expression was higher in HSPC compared to EP following addition of 3 µg/mL Tm (Supplementary Fig. 2c). Thus, the selective enrichment of PERK pathway target genes under basal conditions in HSC is further amplified with Tm treatment.

Since persistent ER stress and UPR signaling can lead to activation of apoptosis through signals downstream of the IRE-1 and PERK branches of the UPR[13], we wanted to determine whether differential UPR branch activation between HSPC and EP influenced cell fate outcome. While Tg treatment did not result in survival differences between HSPC and EP (Supplementary Fig. 3a), Tm treatment significantly reduced CB-derived HSPC survival as compared to EP (HSPC: 33.3±4.1%, EP: 53.0±4.9% at 0.6 µg/mL Tm; HSPC: 2.1±0.4%, EP: 6.4±0.6% at 3

μg/mL Tm, Fig. 2a-b). Adult BM-derived HSPC also showed reduced survival at 3 μg/mL Tm (HSPC: 1.1±0.2%, EP: 16.1±4.4%, Fig. 2b). Cell cycle activation of CB-derived HSPC decreased but did not eliminate the survival difference with EP, suggesting that Tm sensitivity may be partly linked to the inherent quiescence of HSPCs (Supplementary Fig. 3b). Tm reduced the clonogenic capacity of $CD34^{+}CD38^{-}CD45RA^{-}CD90^{+}$ HSC by 19-fold compared to 1.3-fold in EP (Fig. 2c, Supplementary Fig. 3c-d). To determine if the selective loss of HSC following Tm treatment was due to apoptosis, we cultured CB cells with Tm and assessed apoptosis by Annexin-V staining. Although basal levels of viability were similar between HSC and EP, the remaining percentage of viable Annexin-V^{-} cells upon Tm treatment was lower for HSC compared to EP (HSC: 15±3.5%, EP: 47±6.1% after 40 hours, Fig. 2d-e). Increased apoptosis of HSC compared to EP following Tm treatment was confirmed using pre-sorted cells (Supplementary Fig. S3e). Overall, these data indicate that Tm-induced ER stress not only elicits distinct UPR signaling in HSC compared to EP, but also causes selective apoptosis of HSC.

ER stress induces eIF2α phosphorylation (eIF2α~P) by PERK, leading to global translational attenuation but, paradoxically, ATF4 and CHOP translation is increased[14-16]. ATF4 and CHOP can induce apoptosis upon prolonged ER stress, in part by upregulating the eIF2α phosphatase *GADD34*, leading to increased protein load through translational recovery[17,18]. We investigated whether increased apoptosis of HSC compared to EP is linked to preferential upregulation of PERK pathway target genes. First, we constructed a lentiviral ATF4 reporter vector that marks transduced cells with TagBFP while GFP provides a measure for the ATF4 translation rate, which is increased when eIF2α~P is high due to the structure of the 5' end of ATF4 mRNA[14] (Fig. 3a, Supplementary Fig. 4). As expected, Tm treatment increased the ATF4 reporter transgene ratio (TGR) in transduced CB cells (2.47±0.17-fold), an effect that was

inhibited by the PERK inhibitor GSK2606414 (Fig. 3b). In sorted HSPC and EP, the ATF4 reporter TGR was higher in HSPC compared to EP (Fig. 3c-d), consistent with increased baseline level ATF4 translation in HSPC. Following Tm addition, the TGR was more efficiently induced in HSPC compared to EP (HSC: 2.5±0.3 fold, p=0.032; EP: 1.9±0.2 fold, p=0.071, Fig. 3c-d), indicating that Tm stimulates PERK pathway activity more strongly in HSC compared to EP. Second, we over expressed constitutively active GADD34 (ca-GADD34-OE), which prevents eIF2α~P and upregulation of ATF4 and CHOP[19]. Expression of ca-GADD34 significantly increased HSPC survival following Tm treatment (CTRL: 41.0±5.7%, ca-GADD34-OE: 61.0±6.6% at 0.6 μg/mL Tm; CTRL: 2.8±0.8%, ca-GADD34-OE: 10.5±1.1% at 3 μg/mL Tm, Fig. 3e). In EP, the effect did not reach statistical significance (Fig. 3f), indicating that ca-GADD34-OE has a more pronounced effect on the stress response of HSC compared to EP. As a third method to test PERK pathway involvement, we treated sorted HSPC and EP with both Tm and Salubrinal (Sal), which prevents eIF2α dephosphorylation[20]. Without Sal addition, the viability of HSPC was lower than that of EP following Tm treatment (HSPC: 32±3%, EP: 56±2%, Fig. 3g). Addition of Sal and Tm together preferentially increased HSPC survival, resulting in similar viability between HSPC and EP (HSPC: 58±6%, EP: 64±2% at 20 μM Sal), indicating that the differential response between HSC and EP to Tm is dependent on GADD34-mediated dephosphorylation of eIF2α. Fourth, we treated sorted HSPC and EP with both Tm and the PERK inhibitor GSK2606414[21]. Like Sal, GSK2606414 reduced the difference in survival of Tm treatment between HSPC and EP (HSPC: 54.4±1.9%, EP: 58.7±2.5% at 600 nM GSK2606414, Fig. 3h). Thus, HSPC can be protected from Tm-induced apoptosis by interfering with the PERK pathway at multiple junctions, and this equalizes the survival between HSPC and EP. Collectively, these data demonstrate that Tm-induced ER stress preferentially induces

signaling through the PERK branch of the UPR in HSC compared to EP, resulting in selective upregulation of pro-apoptotic genes and increased HSC death.

We next asked whether the UPR was directly involved in regulating HSC function under physiological stress conditions. Since *CHOP* is a main driver of apoptosis upon PERK activation[13,17], the BM of *Chop*$^{-/-}$ mice was analyzed. The frequency of mouse stem and progenitor cells was not significantly changed in *Chop*$^{-/-}$ mice compared to wild-type controls, but there was a small increase in the basal levels of viability of Lin^{-}Sca-1^{+}c-Kit^{+} mouse HSC-enriched cells as well as Lin^{-}Sca-1^{-}c-Kit^{+} progenitors (Supplementary Fig. 5a-b, Supplementary Table 3). This suggests that *Chop* may be required for the survival/death balance of mouse hematopoietic progenitors under physiological conditions. Next, we investigated whether modulating UPR signaling would alter human HSC function. The UPR target gene *ERDJ4* is a co-chaperone that increases the ATPase activity of GRP78 and can be released from the ER membrane to associate with the ERAD machinery[22,23]. These functions may enhance cellular protein folding capacity and protect against UPR-induced apoptosis[24]. *ERDJ4* expression was highest in purified CB-derived CD49f^{+} HSC and was reduced in CD49f^{-} multipotent progenitors (2.0-fold) as well as all EP fractions (2.2- to 4.1-fold, Fig. 4a). GFP-marked *ERDJ4* over expression (ERDJ4-OE) lentiviral vectors were constructed to express different transgene levels (2.3× with PGK-ERDJ4 and 218× with SFFV-ERDJ4, Fig. 4b-c). In the TEX cell line[25], SFFV-ERDJ4 expression decreased Tm-induced apoptosis (Supplementary Fig. 5c-d). Importantly, CB-derived HSPC expressing SFFV-ERDJ4 were also protected from Tm-induced cell death (SFFV-CTRL: 51±4% survival, SFFV-ERDJ4: 62±5% survival, Fig. 4d), suggesting that ERDJ4-OE increases the threshold of ER stress needed to induce apoptosis. To test whether *ERDJ4* influences human HSC function, CB cells were transduced with PGK-ERDJ4 and transplanted

into immune-deficient mice. After 20 weeks of in vivo competition between GFP^+ with GFP^- cells the percentage of GFP^+ cells in the PGK-ERDJ4 group was increased compared to the PGK-CTRL group (PGK-CTRL day 0: 28±3.8%, 20 weeks: 27±5.5%; PGK-ERDJ4 day 0: 44±9.4%, 20 weeks: 70±7.9%; Fig. 4e, Supplementary Fig. 5e). To directly measure the impact of ERDJ4-OE on the function and number of HSC, in vivo limiting dilution analysis (LDA) was performed. PGK-ERDJ4 transduced CB cells were expanded in vitro and sorted GFP^+ cells were injected at limiting cell doses, resulting in higher engraftment compared to CTRL cells (Fig. 4f, Supplementary Fig. 5f-g). The number of mice with human engraftment was also changed: at the low dose, 5 out of 11 control mice were engrafted, compared to 11 out of 12 ERDJ4-OE mice, demonstrating by LDA that there was a 4.4-fold increase in the number of repopulating HSC in the ERDJ4-OE group (CTRL: 1/73137, ERDJ4-OE: 1/16641, Fig. 4g). These data provide strong evidence that a protein folding factor classically associated with the UPR governs HSC function.

To understand the mechanism by which ERDJ4-OE can improve human HSC function, we confirmed that ERDJ4-OE does not change in vivo lineage differentiation, the frequency of phenotypic stem and progenitor cell compartments, homing, or progenitor cell engraftment (Supplementary Fig. 6a-d). This suggests that ERDJ4-OE does not have a strong effect on progenitor cells. As well, secondary LDA showed that ERDJ4-OE does not cause an expansion of functional HSC during repopulation (Supplementary Fig. 6e), indicating that the effects of ERDJ4-OE are transient. To investigate whether ERDJ4-OE protects against ER stress during the in vivo transplantation procedure, *CHOP* and *GADD34* expression was quantified at different time points. In PGK-CTRL transduced CB cells, induction of *CHOP* (2.2±0.6-fold) and *GADD34* (14.4±4.0-fold) expression was seen 19 hours after transplantation compared to before transplantation (Fig. 4h), consistent with a stress response upon transplantation. In contrast, in

PGK-ERDJ4 transduced CB cells, this surge in *CHOP* and *GADD34* expression was absent (0.82±0.18-fold and 0.98±0.06-fold, respectively). These data suggest that ERDJ4-OE improves engraftment by protecting HSC from UPR-induced apoptosis following transplantation. Transplantation of human HSC in the xenograft environment places them under replicative stress, which causes elevated ROS, DNA damage, and loss of HSC function[2]. Since both ROS and DNA damage can cause ER stress, it is possible that these processes are connected to the UPR[5]. In support of this idea, it was recently shown that ROS accumulation leads to UPR-mediated apoptosis of HSC[26]. Our findings implicate ER proteostasis as a critical regulator of HSC function during repopulation and suggest that moderation of UPR activation may have clinical applications if it improves HSC survival during stem cell transplantation.

Our results establish a previously unrecognized link between UPR signaling and human HSC function. The different branches of the UPR are distinctly activated in HSC compared to EP, with the consequence that HSC are rapidly cleared while EP are spared when exposed to various sources of stress. This biological response of human HSC is consistent with the HSC specific induction of apoptosis seen following DNA damage and ROS accumulation[2,27,28]. Collectively, these data reveal an intrinsic biological focus on preventing propagation of damaged HSC that would increase the chance of malignancy. Since terminal differentiation effectively purges damaged progenitor cell progeny, clonal purity may be of less importance in EP. Loss of HSC and intestinal stem cells in mouse models with deletion of the chaperone *Grp78* support the idea that stem cells of multiple tissues can interrogate ER stress, and utilize differential UPR activation to mitigate against potentially pathological damage[29,30]. Overall, our data point to the elimination of individual HSC following stress and damage as a paradigm of how the stem cell pool maintains integrity, thereby ensuring long-term tissue maintenance.

METHODS SUMMARY

CB cells were lineage depleted to enrich for $CD34^+$ cells and then sorted by Fluorescence Associated Cell Sorting, cultured with ER stress-inducing agents, and/or transduced with lentivirus. Quantitative RT-PCR was performed using a 7900 HT Real-Time PCR system, primer sequences are listed in Supplementary Table 2. Apoptosis was assessed by Annexin-V/Sytox or cleaved Caspase-3 staining followed by flow cytometry. Intrafemoral transplantation of human CB cells into immune-deficient mice was used to read out HSC repopulation activity by flow cytometry after 10-20 weeks. Unless otherwise stated, p-values were calculated by two-tailed unpaired Student's t-test. Full Methods are provided in the Supplementary Information.

REFERENCES

1. Geiger, H., de Haan, G. & Florian, M. C. The ageing haematopoietic stem cell compartment. *Nat Rev Immunol* (2013). doi:10.1038/nri3433
2. Yahata, T. *et al.* Accumulation of oxidative DNA damage restricts the self-renewal capacity of human hematopoietic stem cells. *Blood* **118,** 2941–2950 (2011).
3. Jan, M. *et al.* Clonal Evolution of Preleukemic Hematopoietic Stem Cells Precedes Human Acute Myeloid Leukemia. *Science Translational Medicine* **4,** 149ra118–149ra118 (2012).
4. Rossi, D. J., Jamieson, C. H. M. & Weissman, I. L. Stems cells and the pathways to aging and cancer. *Cell* **132,** 681–696 (2008).
5. Rutkowski, D. T. & Kaufman, R. J. A trip to the ER: coping with stress. *Trends Cell Biol.* **14,** 20–28 (2004).
6. Walter, P. & Ron, D. The Unfolded Protein Response: From Stress Pathway to Homeostatic Regulation. *Science* **334,** 1081–1086 (2011).
7. Majeti, R., Park, C. Y. & Weissman, I. L. Identification of a hierarchy of multipotent hematopoietic progenitors in human cord blood. *Cell Stem Cell* **1,** 635–645 (2007).
8. Doulatov, S. *et al.* Revised map of the human progenitor hierarchy shows the origin of macrophages and dendritic cells in early lymphoid development. *Nat Immunol* **11,** 585–593 (2010).
9. Notta, F. *et al.* Isolation of Single Human Hematopoietic Stem Cells Capable of Long-Term Multilineage Engraftment. *Science* **333,** 218–221 (2011).
10. Laurenti, E. *et al.* The transcriptional architecture of early human hematopoiesis identifies multilevel control of lymphoid commitment. *Nat Immunol* **14,** 756–763 (2013).
11. DuRose, J. B., Tam, A. B. & Niwa, M. Intrinsic capacities of molecular sensors of the unfolded protein response to sense alternate forms of endoplasmic reticulum stress. *Mol. Biol. Cell* **17,** 3095–3107 (2006).
12. Lin, J. H. *et al.* IRE1 signaling affects cell fate during the unfolded protein response. *Science* **318,** 944–949 (2007).
13. Tabas, I. & Ron, D. Integrating the mechanisms of apoptosis induced by endoplasmic reticulum stress. *Nature Cell Biology* **13,** 184–190 (2011).
14. Lu, P. D., Harding, H. P. & Ron, D. Translation reinitiation at alternative open reading frames regulates gene expression in an integrated stress response. *JCB* **167,** 27–33 (2004).
15. Vattem, K. M. & Wek, R. C. Reinitiation involving upstream ORFs regulates ATF4 mRNA translation in mammalian cells. *Proc. Natl. Acad. Sci. U.S.A.* **101,** 11269–11274 (2004).
16. Palam, L. R., Baird, T. D. & Wek, R. C. Phosphorylation of eIF2 facilitates ribosomal bypass of an inhibitory upstream ORF to enhance CHOP translation. *J Biol Chem* **286,** 10939–10949 (2011).
17. Marciniak, S. J. *et al.* CHOP induces death by promoting protein synthesis and oxidation in the

stressed endoplasmic reticulum. *Genes & Development* **18,** 3066–3077 (2004).
18. Han, J. *et al.* ER-stress-induced transcriptional regulation increases protein synthesis leading to cell death. *Nature Cell Biology* **15,** 481–490 (2013).
19. Novoa, I., Zeng, H., Harding, H. P. & Ron, D. Feedback inhibition of the unfolded protein response by GADD34-mediated dephosphorylation of eIF2alpha. *JCB* **153,** 1011–1022 (2001).
20. Boyce, M. *et al.* A selective inhibitor of eIF2alpha dephosphorylation protects cells from ER stress. *Science* **307,** 935–939 (2005).
21. Axten, J. M. *et al.* Discovery of 7-methyl-5-(1-{[3-(trifluoromethyl)phenyl]acetyl}-2,3-dihydro-1H-indol-5-yl)-7H-pyrrolo[2,3-d]pyrimidin-4-amine (GSK2606414), a potent and selective first-in-class inhibitor of protein kinase R (PKR)-like endoplasmic reticulum kinase (PERK). *J. Med. Chem.* **55,** 7193–7207 (2012).
22. Shen, Y., Meunier, L. & Hendershot, L. M. Identification and characterization of a novel endoplasmic reticulum (ER) DnaJ homologue, which stimulates ATPase activity of BiP in vitro and is induced by ER stress. *J Biol Chem* **277,** 15947–15956 (2002).
23. Lai, C. W., Otero, J. H., Hendershot, L. M. & Snapp, E. ERdj4 protein is a soluble endoplasmic reticulum (ER) DnaJ family protein that interacts with ER-associated degradation machinery. *J Biol Chem* **287,** 7969–7978 (2012).
24. Kurisu, J. *et al.* MDG1/ERdj4, an ER-resident DnaJ family member, suppresses cell death induced by ER stress. *Genes Cells* **8,** 189–202 (2003).
25. Warner, J. K. *et al.* Direct evidence for cooperating genetic events in the leukemic transformation of normal human hematopoietic cells. *Leukemia* **19,** 1794–1805 (2005).
26. Rouault-Pierre, K. *et al.* HIF-2α Protects Human Hematopoietic Stem/ Progenitors and Acute Myeloid Leukemic Cells from Apoptosis Induced by Endoplasmic Reticulum Stress. *Cell Stem Cell* (2013). doi:10.1016/j.stem.2013.08.011
27. Milyavsky, M. *et al.* A Distinctive DNA Damage Response in Human Hematopoietic Stem Cells Reveals an Apoptosis-Independent Role for p53 in Self-Renewal. *Cell Stem Cell* **7,** 186–197 (2010).
28. Ito, K. *et al.* Regulation of oxidative stress by ATM is required for self-renewal of haematopoietic stem cells. *Nature* **431,** 997–1002 (2004).
29. Heijmans, J. *et al.* ER stress causes rapid loss of intestinal epithelial stemness through activation of the unfolded protein response. *Cell Rep* **3,** 1128–1139 (2013).
30. Wey, S., Luo, B. & Lee, A. S. Acute Inducible Ablation of GRP78 Reveals Its Role in Hematopoietic Stem Cell Survival, Lymphogenesis and Regulation of Stress Signaling. *PLoS ONE* **7,** e39047 (2012).

Acknowledgements We thank D. Ron and D. Rubinsztein for critical assessment of this work; all members of the Dick lab, especially O.I. Gan and E. Lechman, for experimental support and advice; A. Khandani, P. Penttilä and the SickKids-UHN flow facility for technical support; N. Jamal for providing bone marrow samples; Dr. G.R. van den Brink for providing the pLV-ca-GADD34 vector; and Dr. L. Naldini for providing the MA1 vector. Work in the Dick lab is supported by grants from the Canadian Institutes for Health Research, Canadian Cancer Society, Terry Fox Foundation, Genome Canada through the Ontario Genomics Institute, Ontario Institute for Cancer Research with funds from the province of Ontario, a Canada Research Chair and the Ontario Ministry of Health and Long Term Care (OMOHLTC). The views expressed do not necessarily reflect those of the OMOHLTC. Work in the Green lab is supported by Leukemia and Lymphoma Research, Cancer Research UK, the Kay Kendall Leukaemia Fund, the NIHR Cambridge Biomedical Research Centre, the Cambridge Experimental Cancer Medicine Centre, and the Leukemia & Lymphoma Society of America.

FIGURE LEGENDS

Figure 1 | Elevated expression of PERK branch genes of the UPR in HSC compared to EP and further amplification following Tm-induced stress. a, **b**, Enrichment of UPR-related genes in human HSC compared to progenitors. (**a**) $CD49f^{+}$ HSC-enriched genes were analyzed for GO category overrepresentation. Node size represents the number of genes corresponding to that node. White, yellow and orange node color correspond to FDR<0.15, <0.1 and <0.01, respectively. (**b**) Heatmap showing 40 UPR-related genes, derived from nodes in (**a**), with differential expression between HSC and progenitors by expression array (FDR<0.05). **c**-**f**, Expression of key UPR genes in sorted HSPC and EP fractions. mRNA levels of (**c**) PERK pathway components, (**d**) *ATF6*, (**e**) *GRP78* and *GRP94* and (**f**) *IRE1* and spliced *XPB1* were measured by qPCR. Solid arrows indicate some transcriptional relationships. Expression was normalized to the average of *GAPDH*, *ACTB* and *PBGD*. Results are shown as mean±SEM of n=6 CB. **g**, **h**, UPR branch activation depends on cell type and stressor. CB HSPC and EP fractions were sorted and plated in the presence of (**g**) 0.2 μM Tg or (**h**) 0.6 μg/mL Tm. mRNA was isolated after 0.5, 1, 6, 16 and 40 hours to measure mRNA levels of *GRP94*, spliced and total *XBP1*, and *CHOP* by qPCR. DMSO treated controls were the same between (**g**) and (**h**). Expression was normalized to *GAPDH*. Data is shown as mean±SEM of n=3 CB, p-value was calculated based on treated/control cells and indicates differential response between HSPC and EP. HSC: hematopoietic stem cell, MPP: multipotent progenitor, MLP: multilymphoid progenitor, CMP: common myeloid progenitor, GMP: granulocyte macrophage progenitor, MEP: megakaryocyte erythrocyte progenitor. * $p<0.05$, ** $p<0.01$, *** $p<0.001$, **** $p<0.0001$. See also Supplementary Fig. 1-2.

Figure 2 | HSC are predisposed to apoptosis compared to EP following treatment with the ER stress agent Tm. a, **b**, Lower survival of CB- and BM-derived HSPC compared to EP in the presence of Tm. HSC/HSPC and EP were sorted from CB or adult BM and plated in the presence of (**a**) 0.6 µg/mL or (**b**) 3 µg/mL Tm. Viable cell counts as a percentage of DMSO controls are shown. Symbols represents individual samples of which fractions are connected by a black line, the blue line indicates mean±SEM of (**a**) n=16 CB and n=5 BM or (**b**) n=7 CB and n=5 BM. **c**, Reduced clonogenic potential of HSC compared to EP upon Tm treatment. 200 HSC or 140 EP were sorted into methylcellulose containing DMSO or 0.6 µg/mL Tm and colonies were counted 13 days later. Data is shown as mean±SEM of n=4 CB. **d**, **e**, Tm treatment causes higher apoptosis in HSC compared to EP. CB cells were plated with 0.6 µg/mL Tm. Cells were stained for primitive surface markers, Annexin-V and Sytox at different time points. (**d**) Representative flow plots show Annexin-V and Sytox staining. (**e**) Quantification of Annexin-V^- cells is shown as mean±SEM of n=5 CB. p-values indicate different viability between HSC and EP. n.s.: not significant. * $p<0.05$, ** $p<0.01$, **** $p<0.0001$. See also Supplementary Fig. 3.

Figure 3 | HSC are predisposed to UPR-induced apoptosis through PERK-eIF2α-ATF4-CHOP-GADD34 signaling. a, Bidirectional lentiviral reporter vector for ATF4 translation rate. All transduced cells are marked by TagBFP; GFP brightness is a measure of ATF4 mRNA translation, which is regulated by uORFs and depends on eIF2α~P[14]. **b**, ATF4 reporter-transduced CB cells were treated with 0.6 µg/mL Tm and increasing doses of the PERK inhibitor GSK2606414. After 30 hours, the transgene ratio (TGR) between GFP and TagBFP was determined. Results are normalized to DMSO and shown as mean±SEM of n=6 CB except at 600 nM GSK2606414 (n=3). **c**, **d**, Higher ATF4 reporter activity in HSPC compared to EP, especially following Tm treatment. Sorted HSPC and EP were transduced with the ATF4

reporter. After 3 days, 0.6 µg/mL Tm was added to the cells and the TGR was measured 30 hours later. (**c**) Representative flow plots show how ATF4 reporter TGR was calculated. (**d**) Results are shown as mean±SEM of n=4 CB. **e**, **f**, Over expression of constitutively active GADD34 (ca-GADD34 OE) has a more pronounced effect on HSPC compared to EP. (**e**) HSPC and (**f**) EP were sorted and transduced with CTRL or ca-GADD34-OE lentivirus. After 3 days, 0.6 µg/mL Tm was added and viable GFP^+ cells were counted 40 hours later. Counts as a percentage of DMSO controls are shown for n=3 CB. Symbols represent individual CB samples of which CTRL or ca-GADD34-OE transduced cells are connected by a black line, p-values were calculated using paired t-tests. **g**, **h**, Interfering with the PERK pathway at multiple junctions preferentially rescues HSC from apoptosis. Sorted HSPC and EP were plated with 0.6 µg/mL Tm. As well, (**g**) the GADD34 inhibitor Sal or (**h**) the PERK inhibitor GSK2606414 was added at concentrations indicated on the x-axes. The percentage of Annexin-V^-Sytox^- cells after 40 hours is shown as mean±SEM of (**g**) n=5 CB or (**h**) n=4 CB. uORF: upstream open reading frame, TGR: transgene ratio, MFI: mean fluorescence intensity. * $p<0.05$, ** $p<0.01$, *** $p<0.001$, **** $p<0.0001$. See also Supplementary Fig. 4.

Figure 4 | *ERDJ4* over expression protects from Tm-induced apoptosis and increases HSC output and frequency. a, *ERDJ4* expression is highest in HSC. mRNA levels were determined by qPCR in seven sorted CB populations (Supplementary Table 1). Expression was normalized to the mean of *GAPDH* and *ACTB*. p-values were calculated in comparison to $CD49f^+$ HSC. Results are shown as mean±SEM of n=3 CB. **b**, **c**, Lentiviral vectors for overexpression of *ERDJ4* from the PGK promoter (PGK-ERDJ4) or the stronger SFFV promoter (SFFV-ERDJ4). (**b**) Transduced CB cells were assessed for *ERDJ4* expression by qPCR. Expression was normalized to *GAPDH*. Data is shown as mean±SEM of n=2 CB. (**c**) K562 cells were transduced

(>95% GFP^+) and cells were lysed for ERDJ4 protein analysis by western blot. ERK2 is shown as loading control. **d**, ERDJ4-OE protects HSPC from Tm-induced apoptosis. Sorted HSPC were transduced with SFFV-CTRL or SFFV-ERDJ4. After 3 days, 0.6 µg/mL Tm was added to the cells and viable GFP^+ cells were counted 40 hours later. Counts as a percentage of DMSO controls are shown for n=11 CB. Symbols represent individual samples of which SFFV-CTRL or SFFV-ERDJ4 transduced cells are connected by a grey line, p-value was calculated using a paired t-test. **e**, ERDJ4-OE endows CB cells with a competitive advantage. Twenty weeks after injection of PGK-CTRL or PGK-ERDJ4 transduced CB cells, mice were sacrificed. The median GFP% of the human $CD45^+$ graft in the injected femur was normalized to the initial transduction. These normalized values are shown as mean±SEM of n=3 CB with 5 mice per group. **f**, **g**, ERDJ4-OE increases the number of engrafting HSC. PGK-CTRL or PGK-ERDJ4 transduced CB cells were expanded in vitro for 10 days and sorted GFP^+ cells were injected at high and low cell doses. (**f**) Total human $CD45^+GFP^+$ engraftment in the injected femur after 10 weeks. p-value was calculated using the Mann-Whitney test. Pooled data is shown for n=3 CB with 4 mice per group, every symbol represents one mouse. (**g**) HSC frequency was calculated based on the number of engrafted mice. **h**, ERDJ4-OE moderates a surge in *CHOP* and *GADD34* expression after transplantation. PGK-CTRL or PGK-ERDJ4 transduced CB cells were expanded in vitro for 12 days and transplanted into mice. $CD34^+GFP^+$ were sorted and *CHOP* and *GADD34* expression was analyzed by qPCR at the indicated time points pre- and post-transplant (at 19 hours and 1 week post-transplant, all GFP^+ cells were sorted due to cell number constraints). Expression was normalized to *GAPDH*. Data is shown as mean±SEM of n=3 CB. B/NK: B- and NK cell progenitor. * $p<0.05$, ** $p<0.01$, **** $p<0.0001$. See also Supplementary Fig. 5-6.

Figure 1

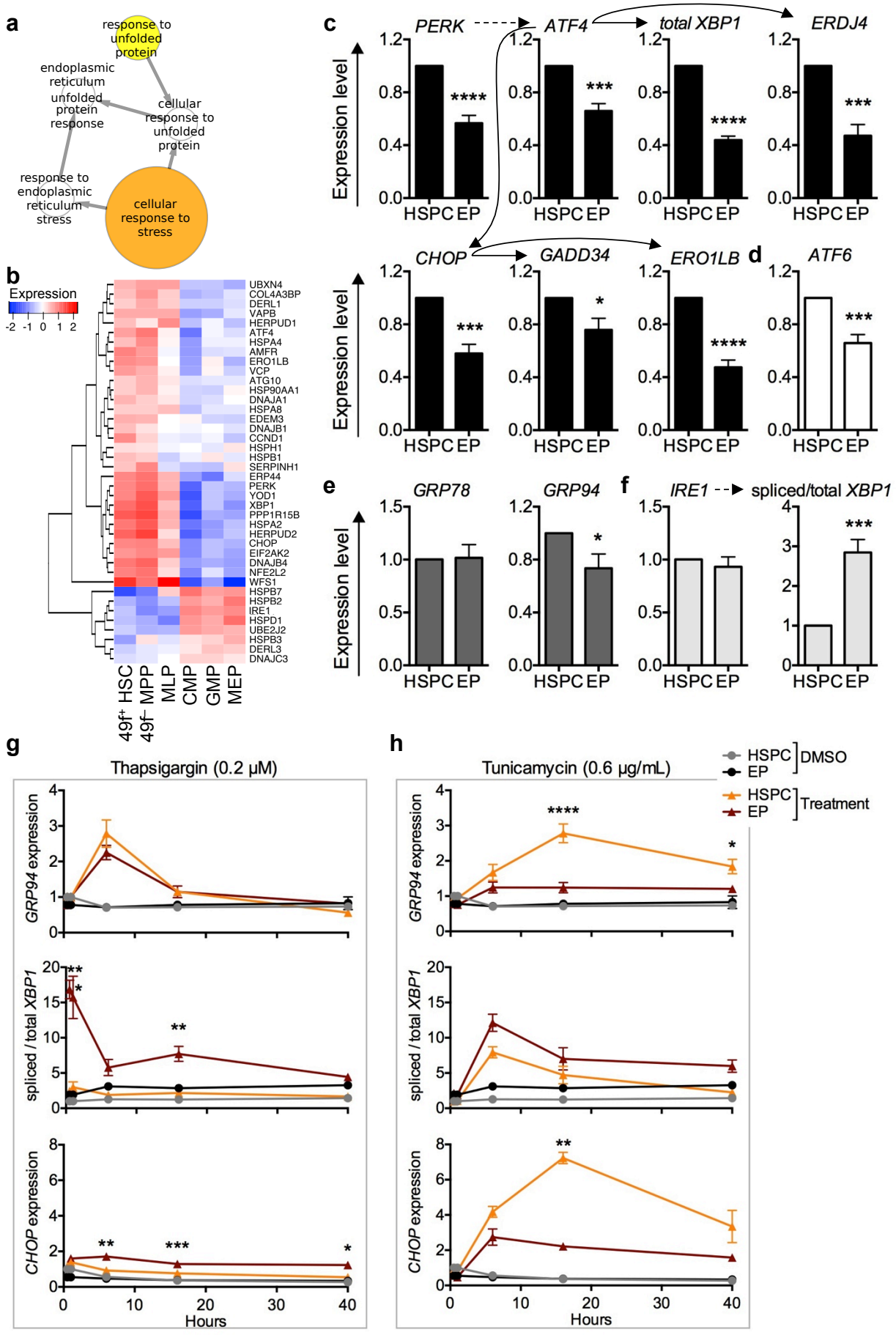
a
response to unfolded protein
endoplasmic reticulum unfolded protein response
cellular response to unfolded protein
response to endoplasmic reticulum stress
cellular response to stress
b
Expression
-2 -1 0 1 2
UBXN4
COL4A3BP
DERL1
VAPB
HERPUD1
ATF4
HSPA4
AMFR
ERO1LB
VCP
ATG10
HSP90AA1
DNAJA1
HSPA8
EDEM3
DNAJB1
CCND1
HSPH1
HSPB1
SERPINH1
ERP44
PERK
YOD1
XBP1
PPP1R15B
HSPA2
HERPUD2
CHOP
EIF2AK2
DNAJB4
NFE2L2
WFS1
HSPB7
HSPB2
IRE1
HSPD1
UBE2J2
HSPB3
DERL3
DNAJC3
49f+ HSC
49f- MPP
MLP
CMP
GMP
MEP
c
PERK
ATF4
total XBP1
ERDJ4
CHOP
GADD34
ERO1LB
d
ATF6
Expression level
HSPC EP
e
GRP78
GRP94
f
IRE1
spliced/total XBP1
g
Thapsigargin (0.2 μM)
GRP94 expression
spliced / total XBP1
CHOP expression
Hours
h
Tunicamycin (0.6 μg/mL)
HSPC
EP
DMSO
Treatment

Figure 2

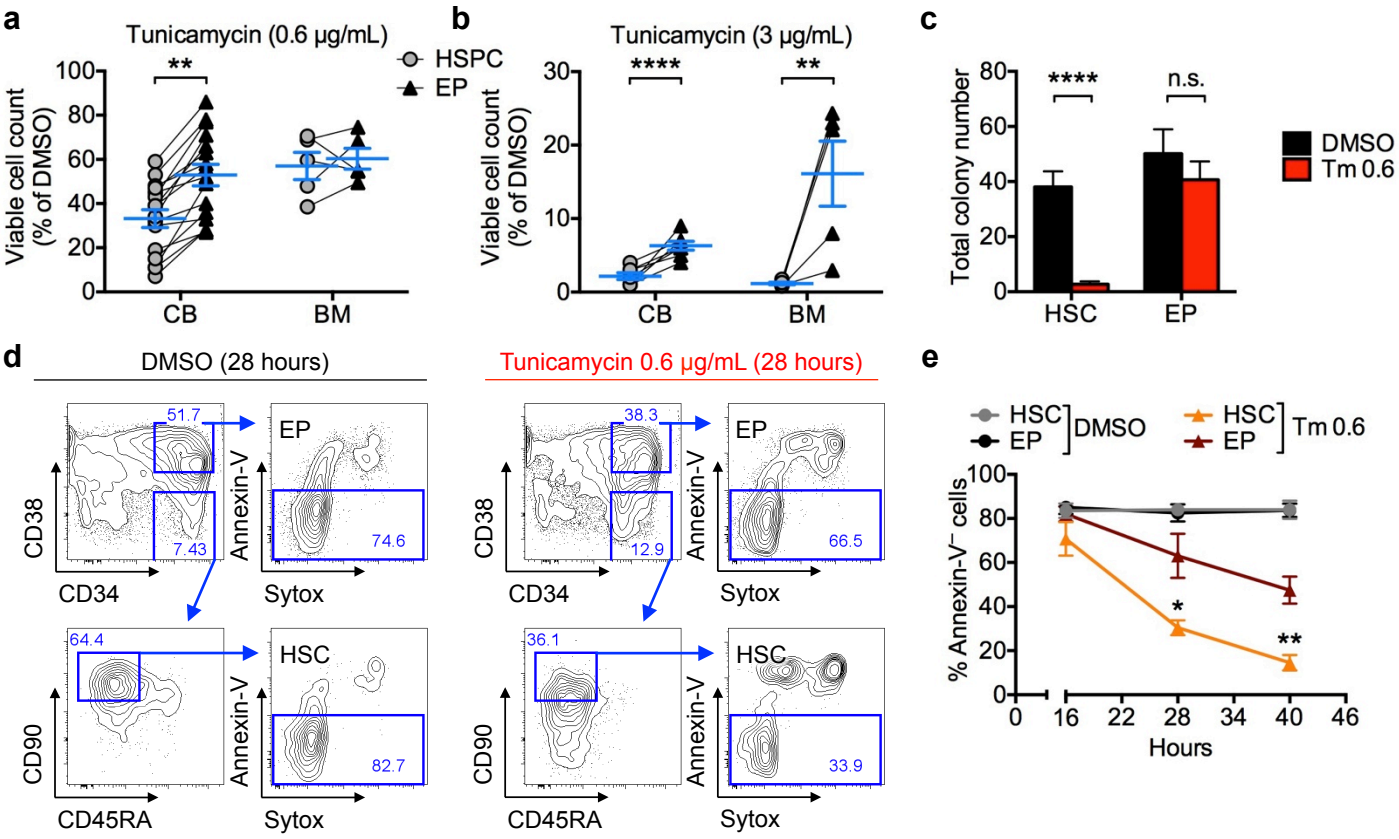
a
Tunicamycin (0.6 µg/mL)
HSPC
EP
Viable cell count (% of DMSO)
**
CB
BM
b
Tunicamycin (3 µg/mL)
****
**
c
Total colony number
****
n.s.
DMSO
Tm 0.6
HSC
EP
d
DMSO (28 hours)
Tunicamycin 0.6 µg/mL (28 hours)
CD38
CD34
Annexin-V
Sytox
CD90
CD45RA
51.7
7.43
74.6
64.4
82.7
38.3
12.9
66.5
36.1
33.9
EP
HSC
e
HSC
EP
DMSO
Tm 0.6
% Annexin-V⁻ cells
Hours
*
**

Figure 3

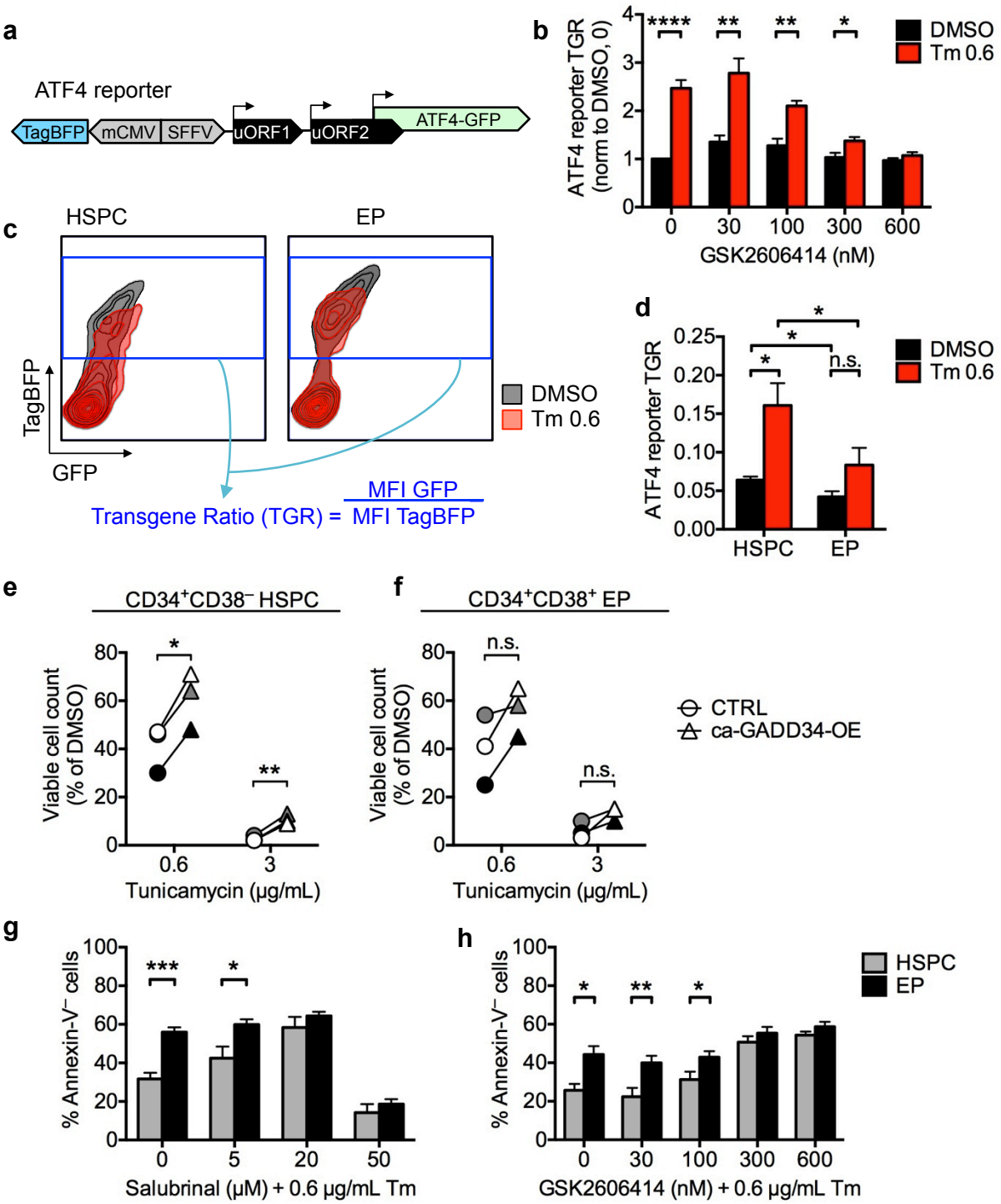
a
ATF4 reporter
TagBFP
mCMV
SFFV
uORF1
uORF2
ATF4-GFP
b
ATF4 reporter TGR (norm to DMSO, 0)
DMSO
Tm 0.6
GSK2606414 (nM)
c
HSPC
EP
TagBFP
GFP
DMSO
Tm 0.6
Transgene Ratio (TGR) = MFI GFP / MFI TagBFP
d
ATF4 reporter TGR
n.s.
HSPC
EP
e
CD34+CD38− HSPC
Viable cell count (% of DMSO)
Tunicamycin (µg/mL)
f
CD34+CD38+ EP
CTRL
ca-GADD34-OE
g
% Annexin-V− cells
Salubrinal (µM) + 0.6 µg/mL Tm
h
HSPC
EP
GSK2606414 (nM) + 0.6 µg/mL Tm

Figure 4

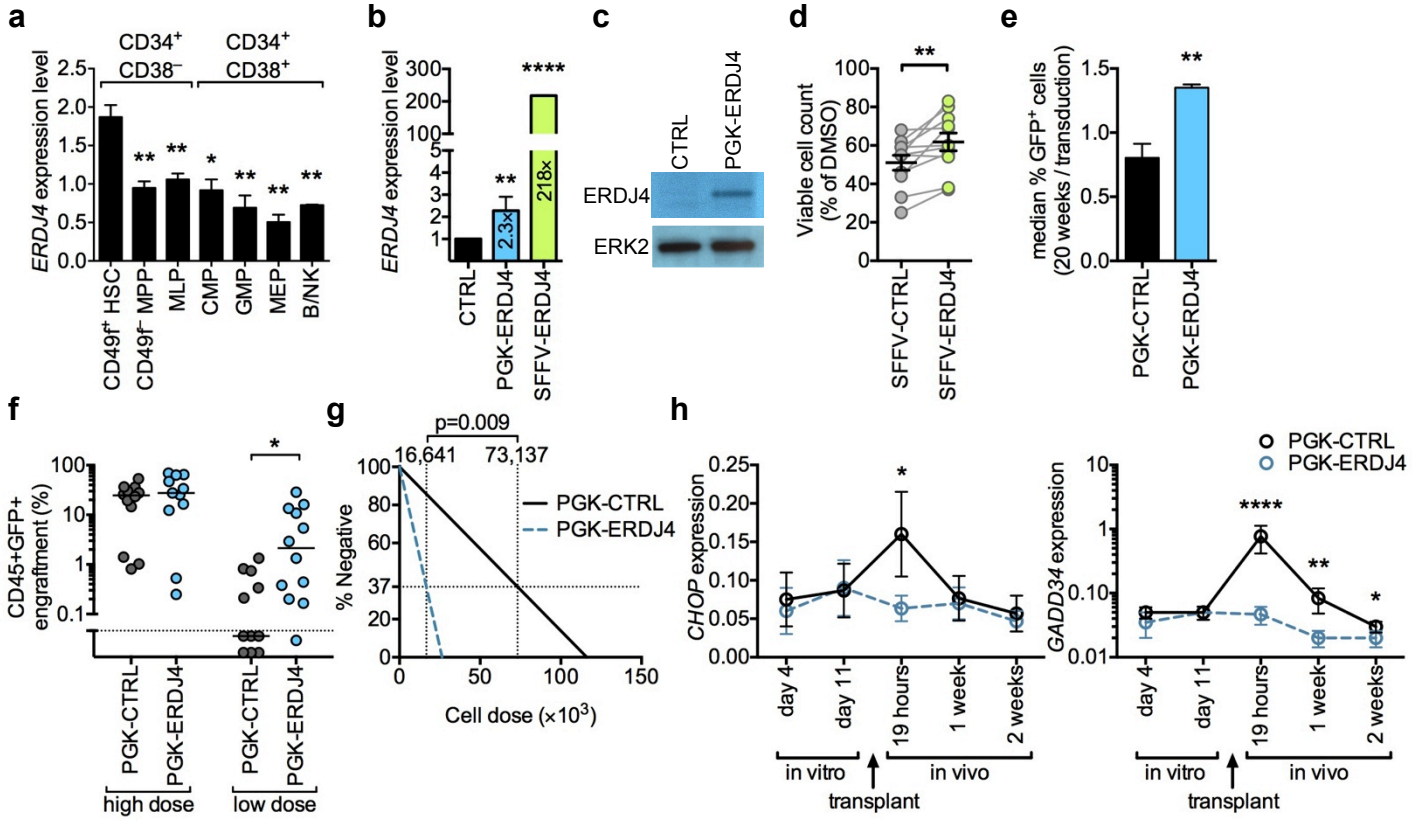
a
CD34+ CD38−
CD34+ CD38+
ERDJ4 expression level
CD49f+ HSC
CD49f− MPP
MLP
CMP
GMP
MEP
B/NK
b
ERDJ4 expression level
2.3x
218x
CTRL
PGK-ERDJ4
SFFV-ERDJ4
c
CTRL
PGK-ERDJ4
ERDJ4
ERK2
d
Viable cell count (% of DMSO)
SFFV-CTRL
SFFV-ERDJ4
e
median % GFP+ cells (20 weeks / transduction)
PGK-CTRL
PGK-ERDJ4
f
CD45+GFP+ engraftment (%)
PGK-CTRL
PGK-ERDJ4
high dose
low dose
g
p=0.009
16,641
73,137
% Negative
PGK-CTRL
PGK-ERDJ4
Cell dose (×10^3)
h
CHOP expression
GADD34 expression
day 4
day 11
19 hours
1 week
2 weeks
in vitro
in vivo
transplant
PGK-CTRL
PGK-ERDJ4

SUPPLEMENTARY INFORMATION

Materials and Methods

Cord blood and bone marrow sample preparation and liquid culture

Umbilical cord blood, bone marrow or mobilized peripheral blood from healthy individuals were obtained with informed consent according to procedures approved by the institutional review boards of the University Health Network and Trillium Hospital. Mononuclear cells were obtained by centrifugation on Ficoll, and lineage depletion was performed using the StemSep Human Progenitor Cell Enrichment Kit according to the manufacturer's protocol (50–75% $CD34^+$, Stemcell Technologies). The lin^- cord blood (CB) or lin^- bone marrow / mobilized peripheral blood cells (BM) cells (50-75% $CD34^+$) were stored in IMDM with 50% FCS and 10% DMSO at -150°C until use. For liquid culture, cells were thawed and plated in X-VIVO 10 (BioWhittaker) supplemented with 1% BSA, 2 mM L-glutamine, 100 U/ml penicillin-streptomycin, and the following cytokines: TPO (7.5 ng/mL), SCF (50 ng/mL), G-CSF (5 ng/mL), Flt3 ligand (50 ng/mL) and IL-6 (5 ng/mL), referred to as TSGF6 culture. The cell line K562 was expanded in IMDM with 10% FCS, 2 mM L-glutamine, 100 U/ml penicillin-streptomycin; TEX cells were cultured as reported previously[1]. Both cell lines tested negative for mycoplasma.

Fluorescence activated cell sorting and flow cytometry

Cells were resuspended at 10^7 cells / mL, stained with surface markers in PBS with 2% FCS, washed and sorted on the BD FACS Aria or MoFlo, consistently yielding >95% purity. Flow cytometry was performed using BD LSRII, BD Canto and BD Fortessa cytometers. Data was analyzed with FlowJo software (Tree Star, Inc.).

Annexin-V/Sytox and cleaved Caspase-3 flow cytometry

For Annexin-V/Sytox apoptosis analysis, cells were stained for surface markers and washed in PBS with 2% FCS, resuspended in binding buffer (diluted 10× in H_2O, BD cat. number 556454) with Annexin-V-APC (50× dilution, BD cat. number 550474) and Sytox Blue (500× dilution, Life Technologies cat. number S34857) and stained for 20 minutes at room temperature. Then the sample was diluted 5× with binding buffer and cells were analyzed by flow cytometry within 60 minutes. For cleaved Caspase-3 analysis, cells were permeabilized for 30 min at room temperature with BD Perm 2 buffer (diluted 10× in H_2O, cat. number 347692), washed in 2 mL PBS with 2% FCS and stained with PE-conjugated cleaved Caspase-3 antibody from BD (cat. number 561011) for 30 minutes at room temperature. Cells were washed again and resuspended in BD Cytofix buffer (diluted 4× in PBS, BD cat. number 554655) before flow cytometry analysis.

Quantitative RT-PCR

RNA was extracted from 500–100,000 cells using TRIzol (Life Technologies) and resuspended in water for cDNA synthesis using the SuperScript III or SuperScript VILO systems according to manufacturer's instructions (Life Technologies). For each qPCR reaction we added 2× Power SYBR Green mix (Life Technologies), 133 nM forward primer and 133 nM reverse primer and RNase-free water up to a total volume of 12.5 µL. cDNA was diluted 6–20× with RNase-free water and 2.5 µL was added for each reaction. The qPCR was performed using a 7900 HT Real-Time PCR system with SDS v2.3 software (Applied Biosystems) using standard settings: 50ºC for 2 min; 95ºC for 10 min; then 95ºC for 15 sec and 60ºC for 1 min repeated for 40 cycles; then dissociation stage. Each assay was run in duplicate for technical variation and for at least 3 CB. Arbitrary mRNA concentrations were calculated using the relative standard curve method, and mRNA concentrations were normalized to *GAPDH*, *PBGD* and/or *ACTB*, as indicated in the fig-

ure legends. To determine *XBP1* splicing levels, primers were designed that amplify all or only spliced *XBP1* mRNA, and spliced *XBP1* expression was divided by total *XBP1* expression (indicated as "spliced / total *XBP1*"). qPCR primer sequences are listed in Supplementary Table 2.

Methylcellulose colony forming assays

Methylcellulose (Stemcell Technologies MethoCult H4034) was supplemented with IL-6 (10 ng/mL), Flt3 ligand (10 ng/mL) and DMSO or Tunicamycin (0.6 µg/mL). Using the BD FACS Aria, 500 $CD34^+CD38^-CD45RA^-CD90^+$ HSC or 350 $CD34^+CD38^+$ EP were deposited in 2.5 mL methylcellulose, and duplicate dishes were plated with 1 mL each (200 HSC or 140 EP per dish). After 13 days, colonies were counted and classified based on morphological appearance.

Lentiviral vectors

The bidirectional lentiviral MA1 vector[2] was modified by replacing ΔNGFR with a loxP-flanked Gateway® cassette (Life Technologies) to generate the destination vector pMAL. To generate PGK-ERDJ4, pMAL was recombined with the *ERDJ4* entry vector from the Mammalian Gene Collection through the PlasmID Repository at Harvard[3] (Clone ID: HsCD00076069). To generate ca-GADD34-OE, the GADD34 fragment was amplified by PCR from the pLV-ca-GADD34 construct[4] using the forward primer 5'-CACCATGGCCAGTGTGCTGG-3' and the reverse primer 5'-TCACTGGGAAGGGAAGAAGG-3', cloned into an entry vector using the pENTR Directional TOPO cloning kit (Life Technologies K2400-20), and this entry vector was recombined with pMAL. To generate SFFV-ERDJ4, the PGK promoter of PGK-ERDJ4 was replaced with the stronger SFFV promoter[5]. Control (CTRL) vectors expressed a humanized *Renilla* Luciferase gene or a Stuffer sequence derived from pLKO.1_1.9Kb_stuffer instead of *ERDJ4* and ca-*GADD34*. The ATF4 reporter lentivirus was made as follows: first, the PGK promoter in pMAL was replaced with the stronger SFFV promoter[5] and GFP was replaced with TagBFP (Evrogen[6])

to generate the destination vector pSMALB. Next, the reporter fragment was amplified from ATF4.5: 5'ATF4.GFP (Addgene 21852), ATF4.12: 5'ATF4.uORF1^{AUA}.GFP (Addgene 21859) and ATF4.14: 5'ATF4.uORF1&2^{AUA}.GFP (Addgene 21861) using the forward primer 5'-CACCAGCTTTTCTGCTTGCTGTC-3' and the reverse primer 5'-TTACTTGTACAGCTCGTC CATGC-3'. Finally, using the pENTR Directional TOPO cloning kit, fragments were cloned into entry vectors, which were then recombined with pSMALB to generate the bidirectional lentiviral reporter vectors pSMALB-ATF4.5rep (hereafter referred to as the ATF4 reporter), pSMALB-ATF4.12rep and pSMALB-ATF4.14rep, respectively. In the ATF4 reporter, mRNA expression highly correlates between TagBFP and GFP due to the bidirectional promoter[2]. To account for differences in basal translation between experimental conditions (such as HSPC vs. EP, high vs. low transduction, DMSO vs. Tm treatment), we calculated the transgene ratio between GFP and TagBFP as a measure of reporter activity:

TGR = GFP mean fluorescence intensity / TagBFP mean fluorescence intensity.

Lentivirus production and primary cell transduction

Viral particles were pseudotyped with the vesicular stomatitis virus G protein using the pMD.G vector and third-generation pMDLg/pRRE and pRSVRev vectors were used for packaging in 293T cells using calcium-phosphate transfection (Clontech cat. number 631312). Lentivirus was concentrated 100× by ultracentrifugation, resuspended in X-VIVO 10 (BioWhittaker) supplemented with 1% BSA and stored at –80ºC until use. CB cells were thawed and plated in liquid TSGF6 culture with double the concentration of all cytokines, and lentiviral suspension was added at a multiplicity of infection of 5-20 in a total volume of 100 µL (96 well plate) or 400 µL (24 well plate). After 16 hours, TSGF6 culture medium was added to expand the cells. Transduction efficiency was measured using flow cytometry for GFP or TagBFP expression after 72-96 hours.

Mouse xenotransplantation, human lin$^-$ cell isolation and secondary transplantation

Mouse xenografts were performed as described previously[7] according to protocols approved by the University Health Network Animal Care Committee. Briefly, 8-12 week old male NOD/Lt-scid/IL2Rγnull (NSG) mice were sub lethally irradiated (225 cGy) 1 day prior to injection. Cells were injected intrafemoral with 30 μL PBS. Peripheral blood (80 μL) was taken from the saphenous vein and analyzed by flow cytometry. Mice with >40% human T cells in the peripheral blood are likely to harbor an auto-immune clonal T-cell expansion and were excluded from analysis. To reach statistical significance, all animal studies were repeated with 3 CB with at least 2, but generally 5 mice per condition. Animals were not randomized prior to injection, no blinding was done for animal studies. After sacrificing the mice, femurs were flushed with 2 mL PBS 2% FCS; 50 μL was stained for surface markers and analyzed by flow cytometry. For lineage depletion, BM cells from the femurs and tibias of 5 mice were combined and processed with the StemSep Mouse/Human Chimera Enrichment Kit (Stem Cell Technologies) according to the manufacturer's instructions. However, during the antibiotin incubation step, an additional 50 μL/mL human hematopoietic progenitor enrichment antibody cocktail from the StemSep Human Progenitor Cell Enrichment Kit was added to deplete human lineage-positive cells. Limiting dilution analysis (LDA) in secondary recipient mice was performed by sorting GFP$^+$ cells from pooled BM of primary mice 10 weeks after transplantation. Secondary mice were injected with 30,000 to 1,000,000 cells and analyzed 10 weeks after transplantation; a secondary mouse was scored as positive if it had >0.01% human engraftment. HSC frequency was estimated using the ELDA software[8] (Extreme Limiting Dilution Analysis, http://bioinf.wehi.edu.au/software/elda/).

Analysis of *Chop*$^{-/-}$ mouse bone marrow

Femurs, tibias and pelvises of 13 week old male *Chop*$^{-/-}$ and wild-type littermates were flushed to isolate BM cells. Five to ten million cells were stained with antibodies against surface markers (HSC panel: lineage markers, c-Kit, Sca-1, CD34 and Flk2. Progenitor panel: lineage markers, c-Kit, Sca-1, CD34, IL7R and FcγII/IIIR, Supplementary Table 3). Next, cells were stained using Annexin-V Pacific Blue conjugate (Biolegend) and 7-AAD according to manufacturer's instructions, and analyzed on a BD Fortessa cytometer.

Tunicamycin, Thapsigargin, Salubrinal, GSK2606414

Compounds were purchased as follows: Tunicamycin (Tm), Sigma-Aldrich, cat. number T7765; Thapsigargin (Tg), Sigma-Aldrich, cat. number T9033; Salubrinal (Sal), Santa Cruz, cat. number SZ202332; GSK2606414, Merck Millipore, cat. number 516535. Powder was resuspended in DMSO and stored at -20° C until use. Final DMSO concentration was always <0.6% and equal between treatment and control groups. Viability analysis was performed after 40 hours of treatment, unless otherwise stated in the figure legend. Viable cells were counted manually by Trypan blue exclusion or automated using the BD Canto flow cytometer high throughput sampler (HTS), by counting the number of Annexin$^-$ and/or Sytox$^-$ cells in a specified volume.

Western blot

Transduced K562 cells were lysed, separated with SDS-PAGE and transferred onto a polyvinylidene fluoride membrane as previously reported[9]. Specific antibody to ERDJ4 (Abnova cat. number H00004189-M09) was detected using secondary HRP-conjugated antibodies (Amersham) and visualized by chemiluminescence (Pierce).

Gene expression and pathway analysis

Gene expression data sets were reported previsously[10]. The genes upregulated in HSC compared to progenitor (MLP/CMP/GMP/MEP) with adjusted p-value <0.01 were used for gene ontology (GO) analyses with BiNGO[11]. The algorithm was used with hypergeometric test, multiple test correction (Benjamini-Hochberg False Discovery Rate - FDR) and using the whole Homo Sapiens annotation as a reference set. Data was visualized with Cytoscape[12]; gene sets linked to the UPR response were unlinked from the rest of the network for presentation. For the heatmap, we checked the expression of all genes belonging to GO categories relative to the UPR response (79 genes belonging to GO_0006986, GO_0034620, GO_0034976, GO_0030968 categories). Forty of these were differentially expressed between HSC and progenitors (FDR <0.05). Their expression levels in HSC, MPP, MLP, CMP, GMP and MEP were mean centered.

Statistical analysis

Unless otherwise stated, mean±SEM values are given and p-values were calculated by two-tailed unpaired Student's t-test. Mann-Whitney tests were performed to compare engraftment levels, since these data do not show a normal distribution. ELDA software was used for statistical analysis of in vivo LDA[8] (http://bioinf.wehi.edu.au/software/elda). * $p < 0.05$, ** $p < 0.01$, *** $p < 0.001$, **** $p < 0.0001$.

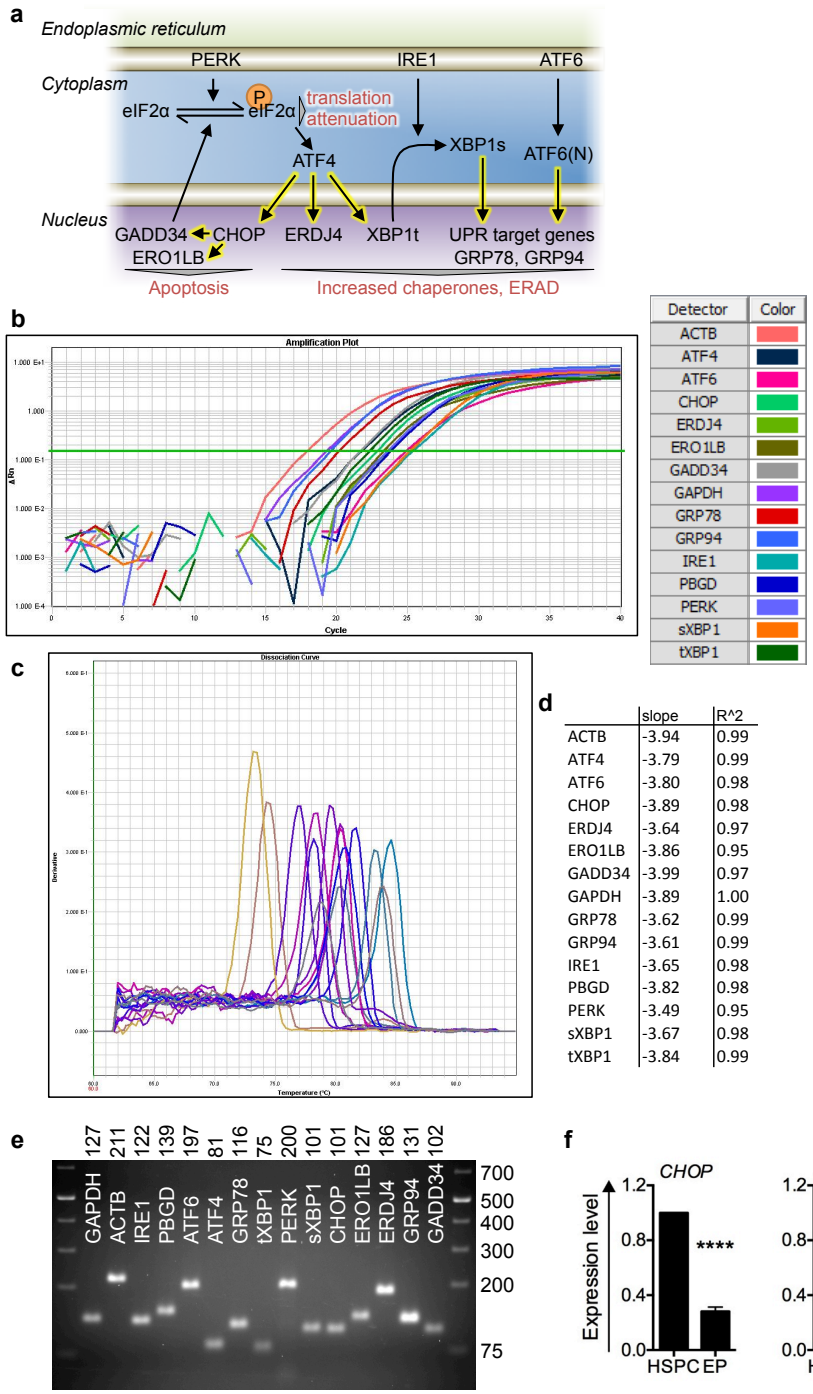

Supplementary Fig. 1 | Expression analysis of UPR-related genes. a, Simplified scheme illustrating UPR signaling events. Three branches of the UPR are activated upon ER stress: IRE-1, PERK and ATF6. IRE-1 splices cytosolic *XBP1* mRNA to enable translation of the XBP1s tran-

scription factor, which upregulates chaperones and ER-associated degradation (ERAD) machinery to resolve ER stress[13]. PERK initiates a different branch of the UPR through phosphorylation of eIF2α, which attenuates global protein synthesis, thus permitting time to restore ER homeostasis[14]. Prolonged ER stress leads to PERK signaling-mediated upregulation of the proapoptotic transcription factor *CHOP* and its target *GADD34*. GADD34 dephosphorylates eIF2α leading to restoration of global protein translation. However, if ER stress is not resolved, *GADD34* upregulation can lead to further accumulation of misfolded proteins, oxidative stress and apoptosis[15]. Yellow highlighted arrows indicate transcriptional regulation. **b,** Amplification curves of qPCR reactions for UPR-related genes. Fluorescence signal during 40 cycles of qPCR reactions on CB-derived cDNA is shown for a representative experiment. Green line indicates threshold that was used to calculate mRNA quantity. **c,** Dissociation curves were generated to check for the presence of aspecific amplicons or primer dimers, which would be visible as additional peaks. Each line represents the dissociation curve of one qPCR reaction, colors indicate different genes. **d,** Slopes and R^2 values of standard curves are shown for a representative experiment. These values were calculated separately for each experiment, based on a cDNA dilution series. **b–d** were performed using SDS v2.3 software. **e,** Agarose gel analysis of qPCR amplicons. qPCR reactions were run on a 3% agarose gel to check for reaction specificity: non-specific amplicons would be visible as additional bands. The expected product size is shown above the gel, the ladder sizes are indicated on the right. **f,** BM cells were sorted into $CD34^+CD38^-$ HSPC and $CD34^+CD38^+$ EP fractions. mRNA levels for *CHOP* and *ERDJ4* were measured by qPCR. Expression was normalized to *GAPDH*. Results are shown as mean±SEM of n=5 BM samples. ERAD: ER-associated degradation. **** $p < 0.0001$.

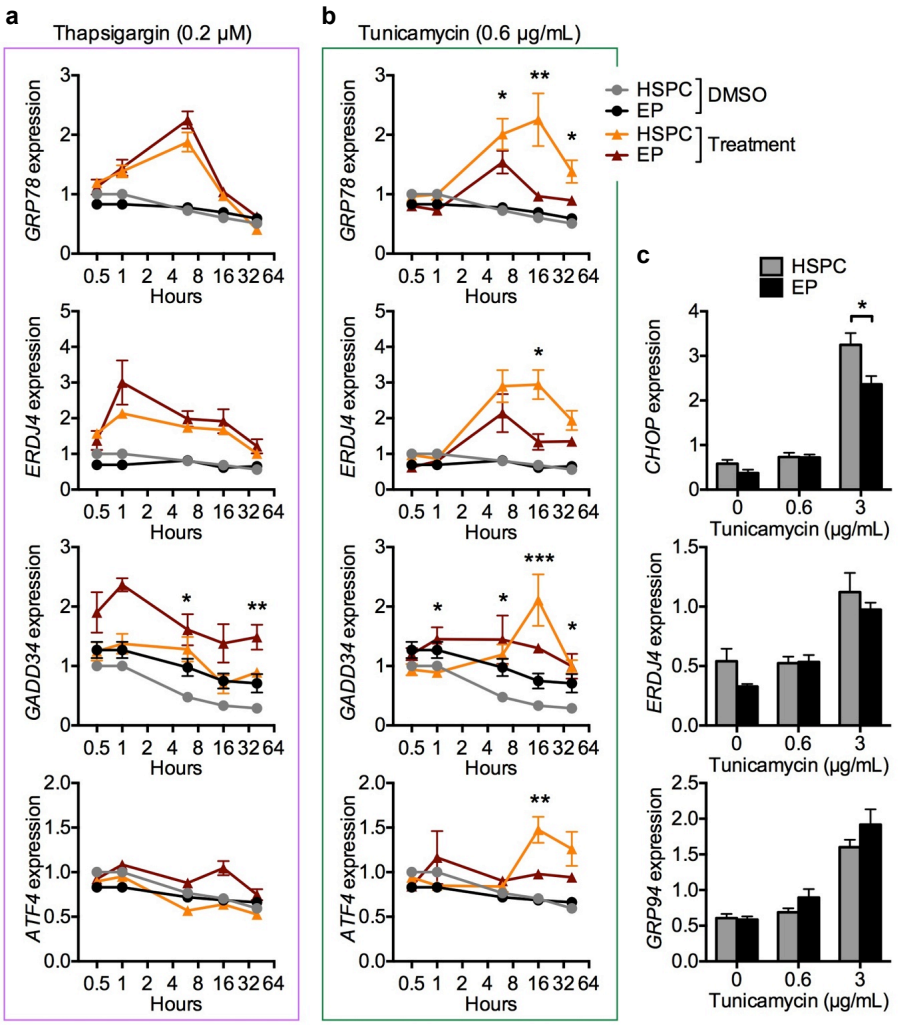

Supplementary Fig. 2 | Differential response of HSPC and EP to ER stress-inducing agents. **a**, **b**, CB HSPC and EP fractions were sorted and plated in the presence of (**a**) 0.2 µM Tg or (**b**) 0.6 µg/mL Tm. mRNA was isolated after 0.5, 1, 6, 16 and 40 hours and expression levels of *GRP78*, *ERDJ4*, *GADD34* and *ATF4* were assessed by qPCR. The DMSO treated controls were the same between (**a**) and (**b**). Expression was normalized to *GAPDH*. Data is shown as mean±SEM of n=3 CB, p-value was calculated based on fold change of treated over DMSO control cells and indicates differential response between HSPC and EP. **c**, BM HSPC and EP were sorted and plated in the presence of 0.6 and 3 µg/mL Tm and DMSO control. After 16 hours, mRNA was isolated and expression levels of *CHOP*, *ERDJ4* and *GRP94* was assessed by qPCR. Expression was normalized to *GAPDH*. Data is shown as mean±SEM of n=5 BM.

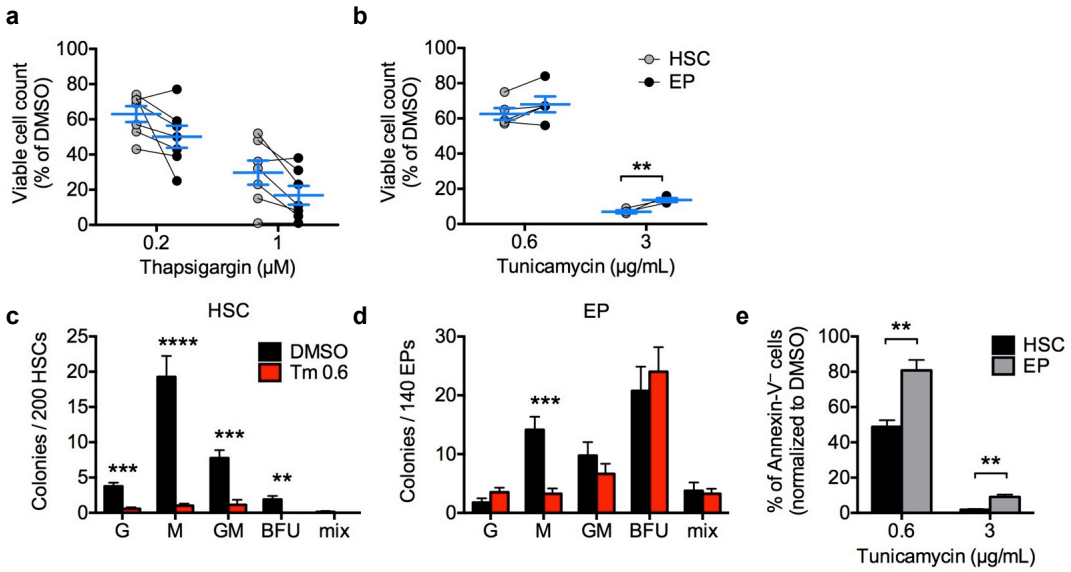

Supplementary Fig. 3 | Survival of HSC is lower than of EP upon Tm, but not Tg treatment. a, Tg has similar toxicity for sorted HSC and EP fractions. Sorted CB HSC and EP fractions were plated in TSGF6 culture conditions in the presence of 0.2 or 1 µM Tg. Viable cell counts as a percentage of DMSO controls are shown as mean±SEM of n=7 CB. **b**, HSC have lower survival than EP following Tm treatment, even after cell cycle induction. Sorted CB HSC and EP fractions were plated in TSGF6 culture conditions with double cytokine concentrations for 72–96 hours to induce G_0 exit of the HSC fraction[7]. Then, cells were plated in the presence of 0.6 or 3 µg/mL Tm. Viable cell counts as a percentage of DMSO controls are shown. Symbols represents individual samples of which fractions are connected by a black line, the blue line indicates mean±SEM of n=5 CB at 0.6 µg/mL and n=3 CB at 3 µg/mL Tm. **c**, **d**, Reduced clonogenic survival of sorted CB HSC compared to EP upon Tm treatment. Total colony number is shown in Fig. 2c. Here, data is separated into colony types based on morphological appearance. Data is shown as mean±SEM of n=4 CB. **e**, Increased apoptosis of sorted HSC compared to EP upon Tm treatment. Sorted CB HSC and EP fractions were plated in the presence of 0.6 or 3 µg/mL Tm. Viable cell counts as a percentage of DMSO controls are shown as mean±SEM of n=4 experiments. ** $p<0.01$, *** $p<0.001$, **** $p<0.0001$. G: granulocyte, M: macrophage, GM: granulocyte/macrophage, BFU: erythroid burst forming unit, mix: multilineage.

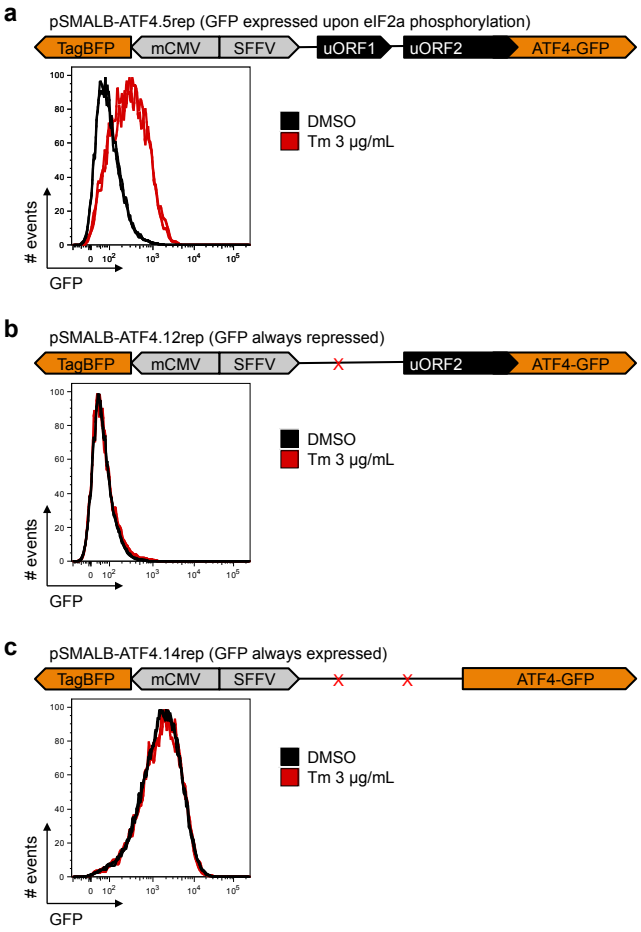

Supplementary Fig. 4 | ATF4 reporter enables visualization of increased ATF4 translation upon Tm treatment. a, ATF4 reporter validation. Two upstream ORFs (uORFs) that are 5' of the ATF4 coding sequence in the ATF4 mRNA ensure more efficient translation of ATF4 when eIF2α phosphorylation levels are high[16,17]. A bidirectional lentiviral vector was constructed that gives constitutive expression of TagBFP to mark transduced cells. In the other direction, the SFFV promoter drives expression of the 5' end of the ATF4 mRNA which fuses with a GFP reporter gene 3' of the termination codon of uORF2. HeLa cells were transduced with pSMALB-ATF4.5rep (hereafter referred to as the ATF4 reporter, >95% transduction efficiency) and treated with Tm at 3 µg/mL. Thirty hours later, GFP fluorescence was read out by flow cytometry. **b**, **c**, Reporter fluorescence depends on uORFs that regulate ATF4 expression. HeLa cells were transduced and treated with Tm at 3 µg/mL. As expected, ATF4-GFP translation is (**b**) repressed in the negative control that has a mutated uORF1 start codon and (**c**) constitutively high in the positive control with mutated start codons for both uORFs[16]. Histogram plots show n=2 technical duplicates (two black lines for DMSO control, two red lines for Tm treatment).

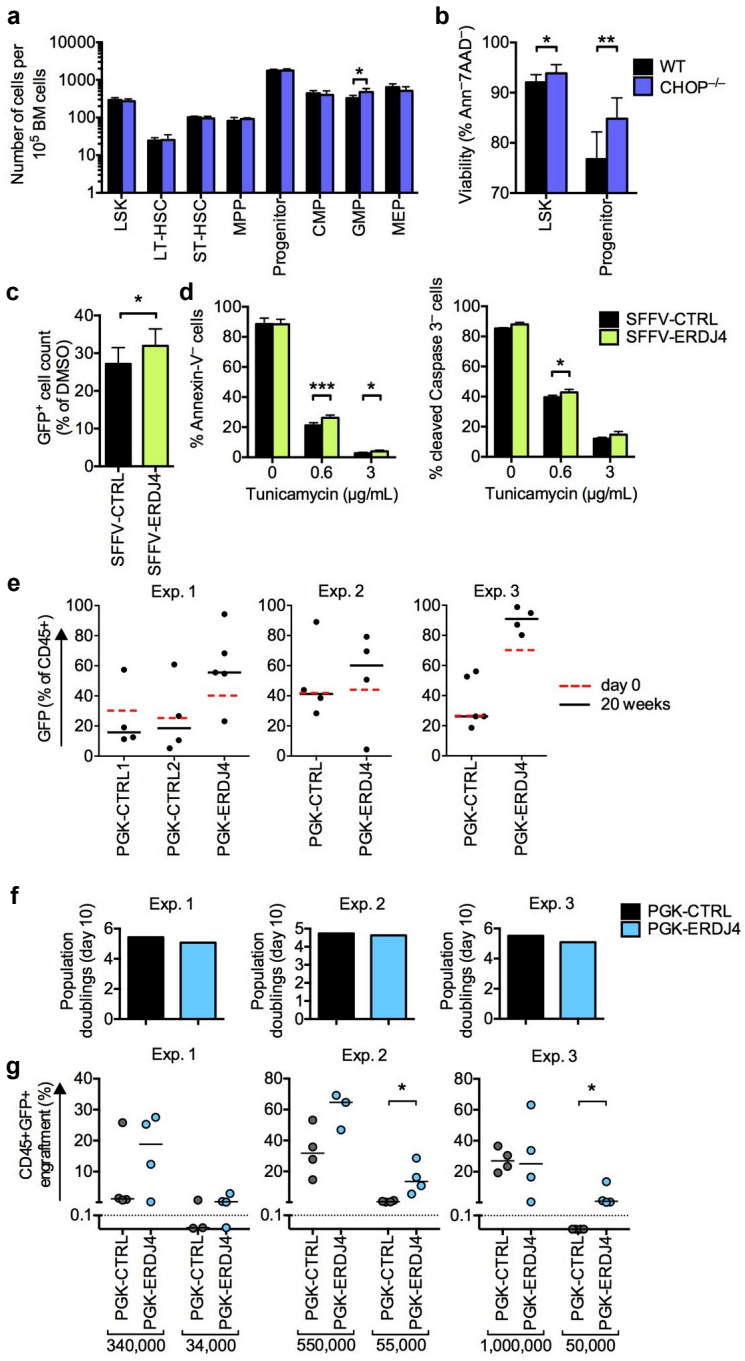

Supplementary Fig. 5 | Modulation of UPR genes affects hematopoietic stem and progenitor cells in vivo. a, Analysis of hematopoietic stem and progenitor cell frequencies in *Chop*$^{-/-}$ mice. Flow cytometry was performed on mouse BM. Each bar graph shows the absolute cell production in each population from wild type or *Chop*$^{-/-}$ mice. Cell numbers are expressed as cells per 100,000 viable BM cells, see Supplementary Table 3 for surface marker overview. Data is shown as mean±SD of n=5 mice per group. **b**, Viability analysis of stem and progenitor cell populations in *Chop*$^{-/-}$ mice. The percentage of viable Annexin-V^{-}7-AAD^{-} cells within the HSC-enriched Lin^{-}Sca-1^{+}c-Kit^{+} (LSK) and Lin^{-}Sca-1^{-}c-Kit^{+} progenitor fractions was assessed by flow cytometry. Data is shown as mean±SD of technical duplicates of n=5 mice per group. **c**, Increased Tm survival or SFFV-ERDJ4 transduced cells. The hematopoietic TEX cell line[1] was transduced with SFFV-

CTRL or SFFV-ERDJ4 and plated in the presence of 0.6 µg/mL Tm. After 48 hours, the number of transduced cells compared to DMSO treated controls was determined by automated counting of GFP^+ cells. Data is shown as mean±SD of n=3 independent experiments. **d**, Tm-induced apoptosis is reduced by SFFV-ERDJ4 transduction. Cells from (**c**) were analyzed for Annexin-V and cleaved Caspase-3 expression by flow cytometry. Data is shown as mean±SD of n=3 independent experiments. **e**, PGK-ERDJ4 endows CB cells with a competitive advantage over untransduced cells. Three CB pools (Exp. 1-3) were transduced with PGK-CTRL or PGK-ERDJ4 lentiviruses and injected into 5 mice each. Dashed line indicates GFP% after transduction (day 0), solid line indicates median GFP% of the human $CD45^+$ graft in the injected femur of xenografted mice (20 weeks). Every symbol represents one mouse. **f**, Similar expansion of PGK-CTRL and PGK-ERDJ4 transduced CB cells in vitro. CB cells were transduced with PGK-CTRL or PGK-ERDJ4 lentivirus and expanded for 10 days in liquid culture. Total population doublings of transduced GFP^+ cells is shown for n=3 CB. **g**, PGK-ERDJ4 increases HSC output. Three CB pools were transduced with PGK-CTRL or PGK-ERDJ4 lentivirus and after 10 days in liquid culture, sorted GFP^+ cells were injected at high and low cell doses, indicated below the x-axis. Total human $CD45^+GFP^+$ engraftment in the injected femur after 10 weeks is shown. p-values were calculated using the Mann-Whitney test. Every symbol represents one mouse, line shows median. Three independent experiments are shown from left to right. LSK: $Lin^-Sca\text{-}1^+c\text{-}Kit^+$, LT-HSC: long-term HSC, ST-HSC, short-term HSC, MPP, multipotent progenitor, CMP, common myeloid progenitor, GMP: granulocyte macrophage progenitor, MEP: megakaryocyte erythrocyte progenitor. * $p < 0.05$, ** $p < 0.01$, *** $p < 0.001$.

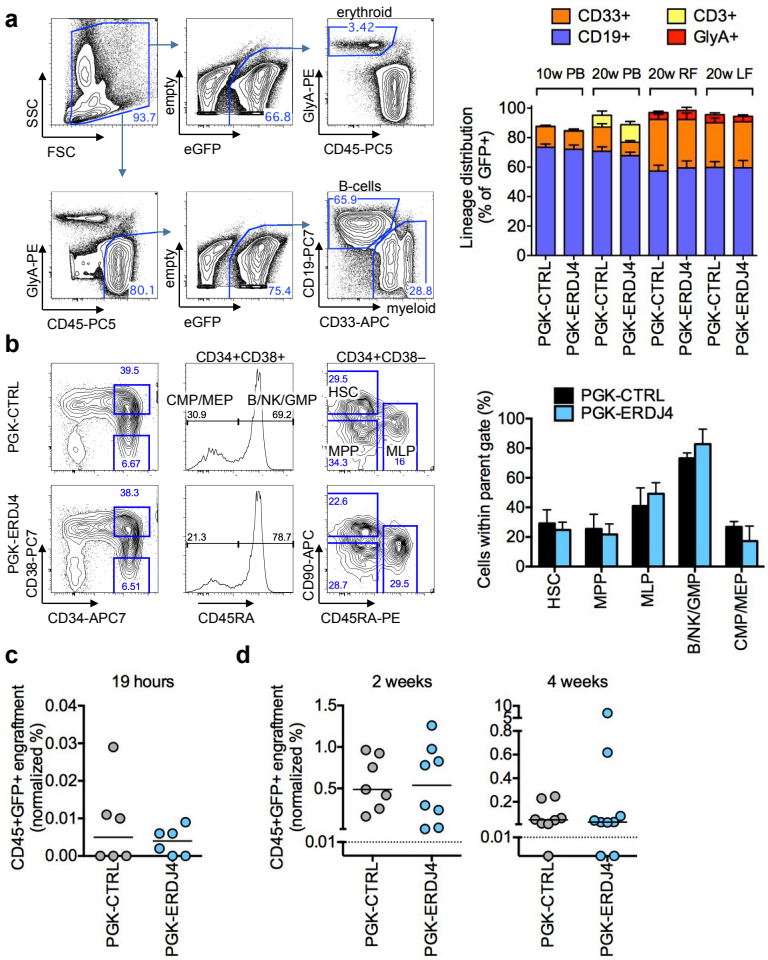

e

	Cell # injected	Engrafted / total mice	HSC frequency 0.95 confidence interval	
PGK-CTRL	1,000,000	7/7 (100%)		
	750,000	2/4 (50%)		
	500,000	1/1 (100%)	Lower:	1 / 886,576
	300,000	0/4 (0%)	Estimate:	1 / 512,185
	250,000	0/3 (0%)	Upper:	1 / 295,895
	200,000	2/4 (50%)		
	100,000	3/5 (60%)		
	30,000	0/3 (0%)		
PGK-ERDJ4	1,000,000	7/7 (100%)		
	750,000	3/4 (75%)		
	500,000	2/4 (50%)	Lower:	1 / 669,112
	300,000	2/4 (100%)	Estimate:	1 / 397,687
	250,000	1/3 (33%)	Upper:	1 / 236,362
	200,000	1/4 (25%)		
	100,000	2/5 (40%)		
	30,000	0/3 (0%)		

Supplementary Fig. 6 | Lineage differentiation, progenitor cell frequencies, homing, EP engraftment, and serial transplantability are maintained upon ERDJ4 over expression. a, PGK-ERDJ4 transduced CB maintains multilineage differentiation potential in vivo. Left: gating scheme to assess differentiation of the human graft in mouse BM. Representative flow plots show quantification of $CD45^+CD19^+$ B-cells, $CD45^+CD33^+$ monocytes and granulocytes, and $CD45^-GlyA^+$ erythroid cells within the GFP^+ graft. Right: the lineage differentiation of CB cells transduced with PGK-CTRL or PGK-ERDJ4 lentiviruses into B cells, myeloid cells, T-cells and erythroid cells was assessed in the peripheral blood (PB) at 10 and 20 weeks and in the injected (RF) and non-injected (LF) femur at 20 weeks after transplantation. Results are shown as mean±SEM of n=15 mice representing n=3 CB. **b**, ERDJ4 over expression (ERDJ4-OE) does not cause aberrant expansion of stem or progenitor cell fractions. To assess the distribution of human stem and progenitor cells, $lineage^+$ and mouse cells were depleted from xenografted mouse BM. The remaining human $lineage^-$ cells

were analyzed by flow cytometry. Left: gating scheme to assess differentiation into HSC, MPP, MLP, CMP/MEP and B/NK/GMP fractions. Right: the frequency of human stem and progenitor cells within the human $CD45^+GFP^+$ graft was assessed 20 weeks after transplantation of PGK-CTRL or PGK-ERDJ4 transduced CB cells. Results are shown as mean±SEM of n=3 CB. **c**, Homing capacity to the non-injected BM is not altered by ERDJ4-OE. PGK-CTRL or PGK-ERDJ4 transduced CB cells were expanded for 12 days in TSGF6 liquid culture conditions and 1E6–1.6E6 cells were transplanted per mouse. After 19 hours, mice were sacrificed to assess human $CD45^+GFP^+$ engraftment in the non-injected femur. Results were normalized to transduction efficiency. Every symbol represents one mouse, results of n=3 CB are shown with 2 mice per group each. **d**, Progenitor cells retain normal engraftment capacity with ERDJ4-OE. Sorted EP were transduced with PGK-CTRL or PGK-ERDJ4 lentivirus and 8,700-14,000 cells were injected per mouse. After 2 and 4 weeks, mice were sacrificed and the level of human $CD45^+GFP^+$ engraftment in the injected femur was measured by flow cytometry. Results were normalized to transduction efficiency. Every symbol represents one mouse, results of n=3 CB are shown with 3 mice per group each. **e**, Frequency of functional human HSC in vivo is maintained with ERDJ4-OE. CB cells were transduced with PGK-CTRL or PGK-ERDJ4 lentivirus and injected into primary mice. After 10 weeks, mice were sacrificed and transduced GFP^+ cells were sorted from their BM. Thirty thousand to one million cells were retransplanted into secondary mice for serial LDA. After 10 weeks, the BM of secondary mice was assessed for human engraftment; mice were scored as positive if the engraftment level was >0.01%. MLP: multilymphoid progenitor, B/NK: B/NK cell progenitor.

Supplementary Table 1 | Surface marker phenotypes to separate human stem and progenitor cells subsets

HSPC	$CD34^+CD38^-$
HSC	$CD34^+CD38^-CD45RA^-CD90^+$
$CD49f^+$ HSC	$CD34^+CD38^-CD45RA^-CD90^+CD49f^+$
MPP	$CD34^+CD38^-CD45RA^-CD90^-$
$CD49f^-$ MPP	$CD34^+CD38^-CD45RA^-CD90^-CD49f^-$
MLP	$CD34^+CD38^-CD45RA^+CD90^{-/lo}$
EP	$CD34^+CD38^+$
CMP/MEP	$CD34^+CD38^+CD45RA^-$
B/NK/GMP	$CD34^+CD38^+CD45RA^+$
CMP	$CD34^+CD38^+CD45RA^-CD10^-CD7^-CD135^+$
MEP	$CD34^+CD38^+CD45RA^-CD10^-CD7^-CD135^-$
B/NK	$CD34^+CD38^+CD45RA^+CD10^+$
GMP	$CD34^+CD38^+CD45RA^+CD10^-CD7^-CD135^+$

HSC: hematopoietic stem cell, MPP: multipotent progenitor, MLP: multilymphoid progenitor, EP: early progenitor, CMP: common myeloid progenitor, MEP: megakaryocyte erythrocyte progenitor, B/NK: B and NK cell progenitor, GMP: granulocyte macrophage progenitor. "HSPC " to "HSC" to "$CD49f^+$ HSC" indicates increasing purity of the population: approximately 1:75, 1:20 and 1:10, respectively[18,19].

Supplementary Table 2 | Primer sequences used for quantitative RT-PCR

Gene	Primer	Sequence 5' to 3'
ACTB	forward	CCTGTACGCCAACACAGTGC
ACTB	reverse	ATACTCCTGCTTGCTGATCC
ATF4	forward	GCTAAGGCGGGCTCCTCCGA
ATF4	reverse	ACCCAACAGGGCATCCAAGTCG
ATF6	forward	ATGAAGTTGTGTCAGAGAACC
ATF6	reverse	CTCTTTAGCAGAAAATCCTAG
CHOP/DDIT3	forward	GGAGCATCAGTCCCCCACTT
CHOP/DDIT3	reverse	TGTGGGATTGAGGGTCACATC
ERDJ4	forward	TCGGCATCAGAGCGCCAAATCA
ERDJ4	reverse	ACCACTAGTAAAAGCAC-
ERO1LB	forward	TTCTGGATGATTGCTTGTGTGAT
ERO1LB	reverse	GGTCGCTTCAGATTAACCTTGT
GADD34/PPP1R15A	forward	CCCAGAAACCCCTACTCATGATC
GADD34/PPP1R15A	reverse	GCCCAGACAGCCAGGAAAT
GRP78/HSPA5/BiP	forward	TGACATTGAAGACTTCAAAGCT
GRP78/HSPA5/BiP	reverse	CTGCTGTATCCTCTTCACCAGT
GRP94/TRA1	Qiagen assay	Qiagen cat. number QT00046963
IRE1/ERN1	forward	TGCTTAAGGACATGGCTACCATCA
IRE1/ERN1	reverse	CTGGAACTGCTGGTGCTGGA
PERK/EIF2AK3	forward	AATGCCTGGGACGTGGTGGC
PERK/EIF2AK3	reverse	TGGTGGTGCTTCGAGCCAGG
PBGD	forward	CATGTCTGGTAACGGCAATG
PBGD	reverse	GTACGAGGCTTTCAATGTTG
XBP1 spliced	forward	CGCTTGGGGATGGATGCCCTG
XBP1 spliced	reverse	CCTGCACCTGCTGCGGACT
XBP1 total	forward	GGCATCCTGGCTTGCCTCCA
XBP1 total	reverse	GCCCCCTCAGCAGGTGTTCC

Supplementary Table 3 | Surface marker phenotypes to separate mouse stem and progenitor cell subsets

Population	
LSK	$Lin^{-}Sca\text{-}1^{+}c\text{-}Kit^{+}$
LT-HSC	$Lin^{-}Sca\text{-}1^{+}c\text{-}Kit^{+}Flk2^{-}CD34^{-}$
ST-HSC	$Lin^{-}Sca\text{-}1^{+}c\text{-}Kit^{+}Flk2^{-}CD34^{+}$
MPP	$Lin^{-}Sca\text{-}1^{+}c\text{-}Kit^{+}Flk2^{+}CD34^{+}$
Progenitor	$Lin^{-}Sca\text{-}1^{-}c\text{-}Kit^{+}$
CMP	$Lin^{-}Sca\text{-}1^{-}c\text{-}Kit^{+}FcγII/IIIR^{-}CD34^{+}$
GMP	$Lin^{-}Sca\text{-}1^{-}c\text{-}Kit^{+}FcγII/IIIR^{+}CD34^{+}$
MEP	$Lin^{-}Sca\text{-}1^{-}c\text{-}Kit^{+}FcγII/IIIR^{-}CD34^{-}$

LT-HSC: long-term hematopoietic stem cell. ST-HSC: short term hematopoietic stem cell. MPP: multipotent progenitor. CMP: common myeloid progenitor. GMP: granulocyte macrophage progenitor. MEP: megakaryocyte erythrocyte progenitor.

References

1. Warner, J. K. *et al.* Direct evidence for cooperating genetic events in the leukemic transformation of normal human hematopoietic cells. *Leukemia* **19,** 1794–1805 (2005).
2. Amendola, M., Venneri, M. A., Biffi, A., Vigna, E. & Naldini, L. Coordinate dual-gene transgenesis by lentiviral vectors carrying synthetic bidirectional promoters. *Nat Biotechnol* **23,** 108–116 (2005).
3. Gerhard, D. S. *et al.* The status, quality, and expansion of the NIH full-length cDNA project: the Mammalian Gene Collection (MGC). *Genome Research* **14,** 2121–2127 (2004).
4. Heijmans, J. *et al.* ER stress causes rapid loss of intestinal epithelial stemness through activation of the unfolded protein response. *Cell Rep* **3,** 1128–1139 (2013).
5. Gentner, B. *et al.* Stable knockdown of microRNA in vivo by lentiviral vectors. *Nat Meth* **6,** 63–66 (2009).
6. Subach, O. M. *et al.* Conversion of red fluorescent protein into a bright blue probe. *Chem. Biol.* **15,** 1116–1124 (2008).
7. van Galen, P. *et al.* Reduced lymphoid lineage priming promotes human hematopoietic stem cell expansion. *Cell Stem Cell* **14,** 94–106 (2014).
8. Hu, Y. & Smyth, G. K. ELDA: extreme limiting dilution analysis for comparing depleted and enriched populations in stem cell and other assays. *Journal of Immunological Methods* **347,** 70–78 (2009).
9. O'Brien, C. A. *et al.* ID1 and ID3 regulate the self-renewal capacity of human colon cancer-initiating cells through p21. *Cancer Cell* **21,** 777–792 (2012).
10. Laurenti, E. *et al.* The transcriptional architecture of early human hematopoiesis identifies multilevel control of lymphoid commitment. *Nat Immunol* **14,** 756–763 (2013).
11. Maere, S., Heymans, K. & Kuiper, M. BiNGO: a Cytoscape plugin to assess overrepresentation of gene ontology categories in biological networks. *Bioinformatics* **21,** 3448–3449 (2005).
12. Lopes, C. T. *et al.* Cytoscape Web: an interactive web-based network browser. *Bioinformatics* **26,** 2347–2348 (2010).
13. Yoshida, H., Matsui, T., Yamamoto, A., Okada, T. & Mori, K. XBP1 mRNA is induced by ATF6 and spliced by IRE1 in response to ER stress to produce a highly active transcription factor. *Cell* **107,** 881–891 (2001).
14. Harding, H. P., Zhang, Y. & Ron, D. Protein translation and folding are coupled by an endoplasmic-reticulum-resident kinase. *Nature* **397,** 271–274 (1999).
15. Marciniak, S. J. *et al.* CHOP induces death by promoting protein synthesis and oxidation in the stressed endoplasmic reticulum. *Genes & Development* **18,** 3066–3077 (2004).
16. Lu, P. D., Harding, H. P. & Ron, D. Translation reinitiation at alternative open reading frames regulates gene expression in an integrated stress response. *JCB* **167,** 27–33 (2004).
17. Vattem, K. M. & Wek, R. C. Reinitiation involving upstream ORFs regulates ATF4 mRNA translation in mammalian cells. *Proc. Natl. Acad. Sci. U.S.A.* **101,** 11269–11274 (2004).
18. Majeti, R., Park, C. Y. & Weissman, I. L. Identification of a hierarchy of multipotent hematopoietic progenitors in human cord blood. *Cell Stem Cell* **1,** 635–645 (2007).
19. Notta, F. *et al.* Isolation of Single Human Hematopoietic Stem Cells Capable of Long-Term Multilineage Engraftment. *Science* **333,** 218–221 (2011).